Check for updates

MOF/COF hybrids as next generation materials for energy and biomedical applications

Cigdem Altintas, [iD]†[a] Ilknur Erucar [iD]†[b] and Seda Keskin [iD]*[a]

The rapid increase in the number and variety of metal organic frameworks (MOFs) and covalent organic frameworks (COFs) has led to groundbreaking applications in the field of materials science and engineering. New MOF/COF hybrids combine the outstanding features of MOF and COF structures, such as high crystallinities, large surface areas, high porosities, the ability to decorate the structures with functional groups, and improved chemical and mechanical stabilities. These new hybrid materials offer promising performances for a wide range of applications including catalysis, energy storage, gas separation, and nanomedicine. In this highlight, we discuss the recent advancements of MOF/COF hybrids as next generation materials for energy and biomedical applications with a special focus on the use of computational tools to address the opportunities and challenges of using MOF/COF hybrids for various applications.

1. Background

Open framework materials have been central to coordination chemistry research since the discovery of zeolites.[1–3] The promise to utilize a wide variety of these structures for various applications including catalysis, ion exchange, and gas separation has accelerated the research on the discovery of novel classes of porous solids with a targeted topology, architecture, crystallinity, and porosity. Metal organic frameworks (MOFs), crystalline structures obtained through the combination of metal nodes and organic ligands in particular topologies, are a result of such efforts devoted to extending the utilization of open framework materials.[4,5] Due to their well-defined distribution of pore sizes and large surface areas (up to $\sim$10 000 m^2 g^{-1})[6] in addition to the ability to tune the chemical functionality of structures during the synthesis, MOFs have been studied for various applications since their discovery at the end of the 1990s.[7,8] However, chemical, thermal, mechanical stabilities of MOFs have been a source of concern, and significant efforts have been devoted for increasing their resistance to degradation under different/harsh chemical conditions.[9]

Soon after witnessing the promises of MOFs, covalent organic frameworks (COFs), obtained *via* covalent bonding of light elements (carbon, nitrogen, oxygen, silicon, and boron), have received significant attention.[10,11] Since 2005, COFs have been considered as an innovative class of porous materials with low densities and high stability in various chemical environments, such as acidic environments,[12–14] and similar to MOFs they are widely studied for gas adsorption, catalysis, and sensing applications. High visible light absorption, high chemical stability, and defect-free structures of COFs make them efficient photocatalysts for the treatment of wastewater, water splitting, and CO$_2$ reduction.[15] Due to their robust structures and nonmetallic features, COFs are also studied as effective nano-agents for cancer treatment.[16]

Both MOFs and COFs have been mostly investigated for adsorption of various types of gas and liquid molecules, such as hydrocarbons, volatile organic compounds, ions, water, dyes, drug solutions, and for the catalysis of different reactions including hydrogenation and oxidation.[17,18] Both families of materials can replace the traditional porous materials for a variety of applications, as long as the bottlenecks of stability, processability, and large-scale production are overcome.[17] The number of experimentally synthesized MOFs in Cambridge Structural Database ($\sim$100 000)[19] is significantly higher than that of COFs (648) reported in the CURATED (Clean, Uniform, Refined with Automatic Tracking from Experimental Database) COF database.[20,21] The range of pore sizes (2.4–72 Å for MOFs and 1.1–56 Å for COFs), surface areas (up to $\sim$8000 m^2 g^{-1}

[a] Department of Chemical and Biological Engineering, Koc University, Rumelifeneri Yolu, Sariyer, 34450, Istanbul, Turkey. E-mail: skeskin@ku.edu.tr; Tel: +90 (212) 338 1362

[b] Department of Natural and Mathematical Sciences, Faculty of Engineering, Ozyegin University, Cekmekoy, 34794, Istanbul, Turkey

† These authors contributed equally to this work.

for MOFs and up to 8500 m^2 g^{-1} for COFs) and porosities (0.2–0.97 for MOFs and 0.25–0.95 for COFs) reported for the MOFs and COFs in recent computation-ready experimental MOF database (CoRE) MOF[22] and CURATED COF database[20] are mostly similar to each other. COFs are generally lighter than MOFs (densities range between 0.1–1.76 g cm^{-3} for COFs and 0.06–7.5 g cm^{-3} for MOFs) and MOFs offer a wider variety of chemical environments compared to COFs thanks to the various types of metal nodes in their structures.

Energy storage	Nanomedicine	Membrane-based separation	Detection of chemicals	Catalysis	Others (e.g. gas capture)
6	7	8	10	28	14

MOF@COF core-shell photocatalytic degradation of Rhodamine B[35]
2018

MOF@COF fillers in mixed matrix membranes for CO_2/CH_4 separation[37]
2019

Bacterial inhibition with MOF@COF nanoenzyme[39]
2020

Bifunctional MOF@COF biomarker sensing and immobilizing HIV-1 DNA[42]
2021

2019 MOF/COF biosensors[36]

2021 COF growth on MOF computational algorithm[40]

2021 MOF-in-COF molecular sieving membrane[41]

2022 MOF@COF for Li-S battery[43]

2016 the first MOF/COF composite membrane-based H_2/CO_2 separation[34]

MOF membrane
interlayer
COF membrane

2020 MOF@COF catalyst with size-selective activity[38]
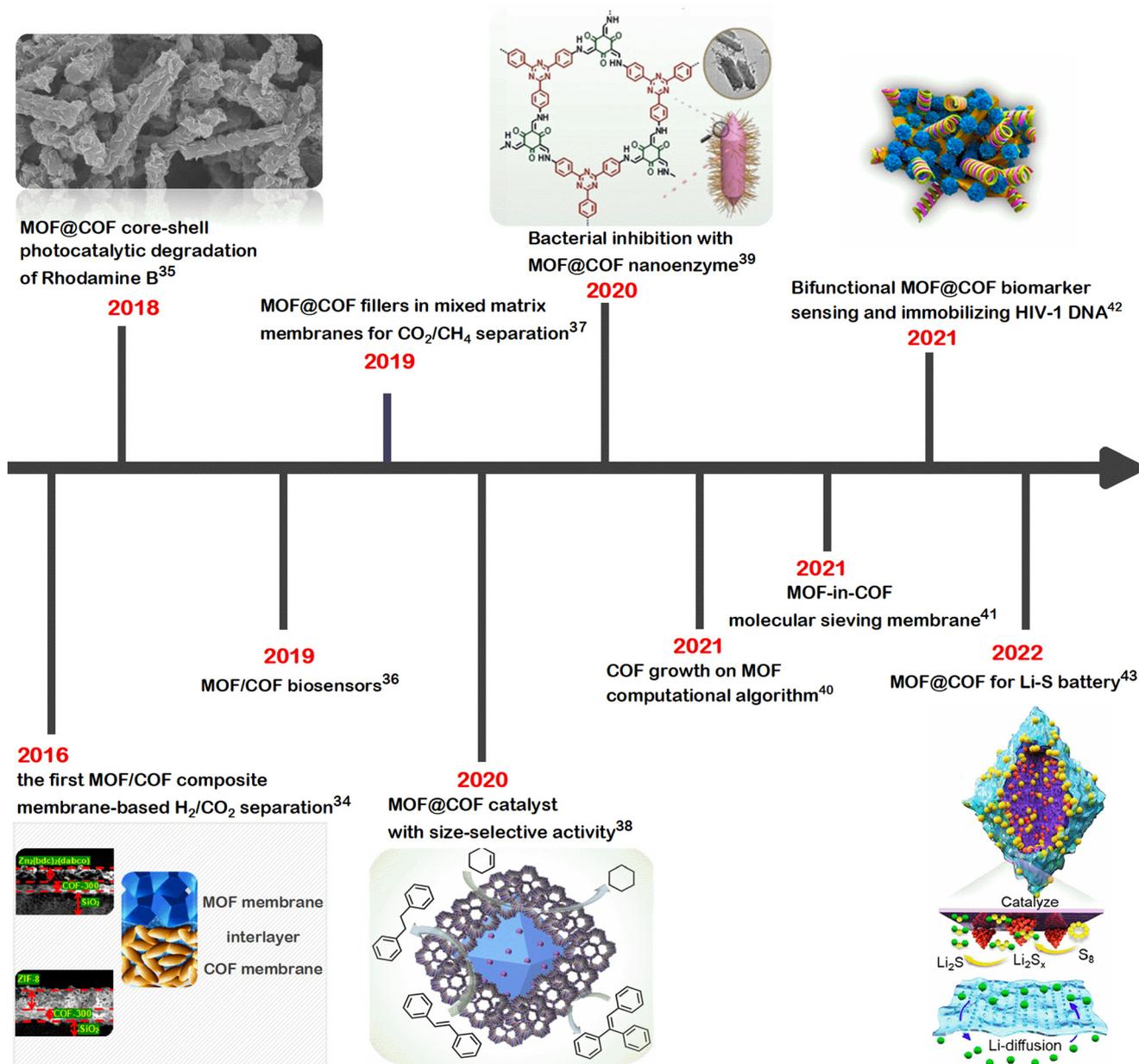
Catalyze
Li_2S Li_2S_x S_8
Li-diffusion

Fig. 1 Main application areas of MOF/COF composites (top). Data was obtained by searching the publications on the Web of Science (as of September 17, 2022), having keywords "metal–organic framework" or "MOF" and "covalent organic framework" or "COF", "hybrid" or "hetero" or "composite". Review articles were excluded. The numbers in each box represent the total number of studies in the corresponding field. Timeline of the representative studies on MOF/COF composites (bottom).[34–43] Figures reprinted with permissions from ref. 34, 35, 38, 39, 42 and 43.

MOF/COF hybrid structures have been recently synthesized as core–shell structures (MOF@COF or COF@MOF), heterostructures, and composites.[23] MOF@COF structures are constructed by covalently bonding COFs to the surface functional groups of MOFs whereas in COF@MOF structures, MOFs are grown on the surface of COFs. For heterostructures like a COF-in-MOF structure, MOFs are used as templates and the COF is grown inside the MOF.
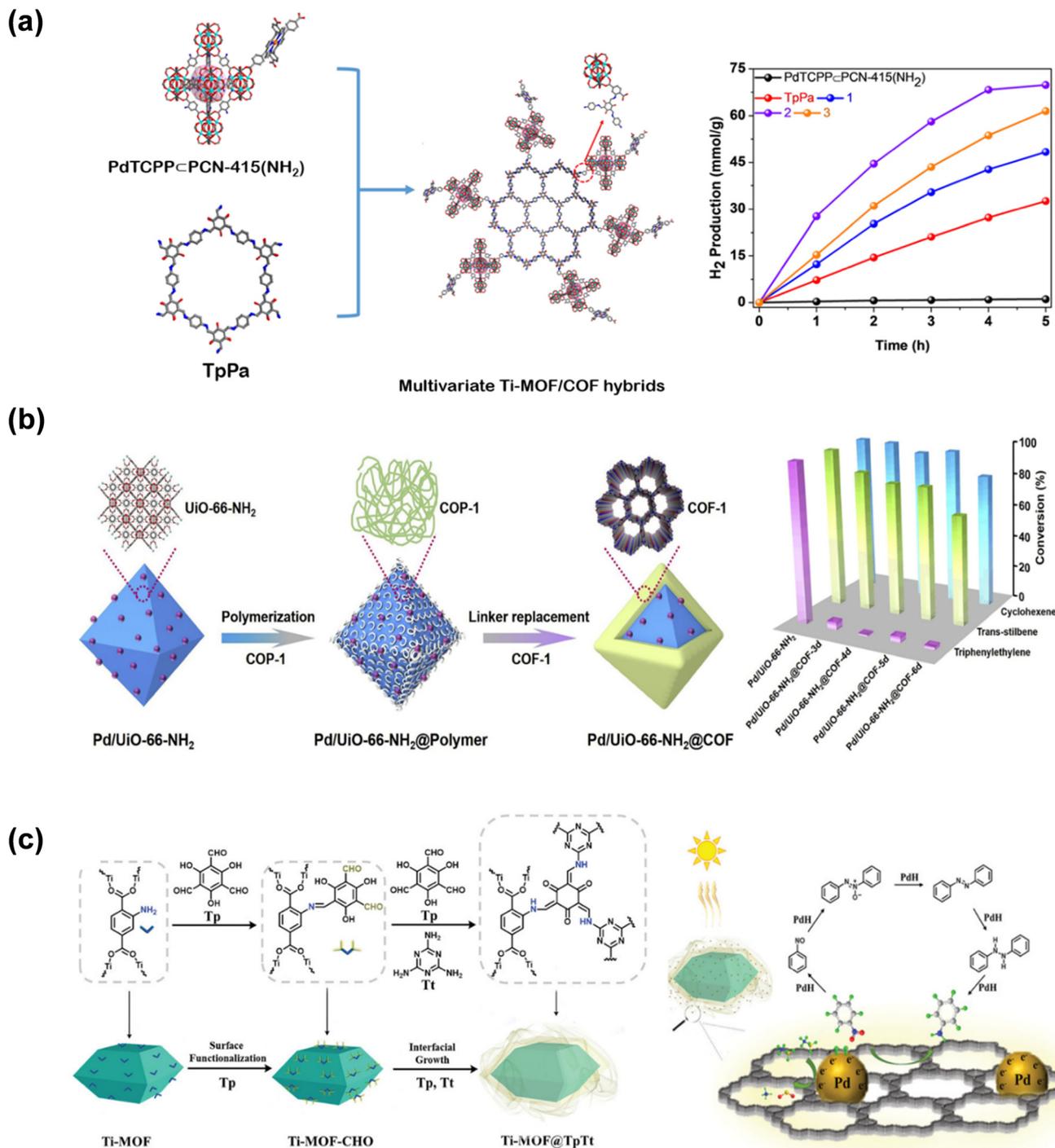

Fig. 2 (a) Schematic representation of multivariate Ti-MOF/COF hybrids (left). Photocatalytic H_2 evolution activity (purple) in the presence of 1.2 wt% Pt cocatalyst. Blue, purple, orange represent Ti-MOF/COF composites 1, 2, and 3, respectively (right). Readapted with permission from ref. 50. Copyright 2021 Wiley-VCH GmbH. (b) Preparation of sandwiched Pd/UiO-66-NH$_2$@COF (left) and its catalytic activity for the liquid-phase hydrogenation of cyclohexene, *trans*-stilbene, and triphenylethylene (right) where MOF@COF-3d, 4d, 5d, and 6d represent the composite samples heated at 120 °C for 3, 4, 5, and 6 days, respectively. Reprinted from ref. 38. Copyright (2020) with permission from Elsevier. (c) Core–shell structure of Pd decorated Ti-MOF@TpTt (left) and nitrobenzene hydrogenation with the core–shell cascade catalyst under visible light (right). Reprinted from ref. 51 under the terms of the CC BY licence **https://creativecommons.org/licenses/by/4.0/**.

Composites, generally represented as MOF + COF, are fabricated using a post-synthetic modification approach where MOF nanoparticles are dispersed on COF sheets.[24] Details of several design strategies from the viewpoint of crystal engineering such as imine formation, boron–oxygen formation, direct condensation, post-synthetic modification, π–π stacking, MOF-in-COF assembly, and modular total synthesis for MOF/COF hybrids can be found in a recent review,[25] and the details of different approaches for synthesizing a target MOF/COF hybrid structure can be found in recent reviews.[2,3,26,27]

Since 2016, MOF/COF hybrids have been examined for a wide range of applications. For instance, the synergy of MOFs and COFs was utilized for adsorption-based wastewater treatment, where problems with the chemical stability of MOFs in aqueous, acidic, and alkaline environments were overcome with the high chemical stability of the COF dispersed on the surface of the MOF.[28] Fig. 1 shows the distribution of the main application areas of MOF/COF hybrids and the timeline of the pioneering works on the utilization of MOF/COF hybrids. Recent comprehensive reviews show that the number of works on these composite materials is rapidly increasing,[2,3,13,23–26,29–33] and MOF/COF hybrids have already been utilized in various applications such as for energy storage,[2] photocatalysis,[26] or biosensing.[33] In this highlight, our aim is to provide a concise and critical overview of the advancements in the applications of MOF/COF hybrids with a special emphasis on the use of computational tools to uncover their potentials.

2. Applications of MOF/COF hybrids

Catalysis

MOFs have been investigated for catalytic applications since the 2000s,[44,45] while the use of COFs in catalysis started later on.[46] Performances of MOF- and COF-based catalysts have signaled that utilizing MOF/COF hybrids in catalytic applications could offer more.[47–49] Most of the studies focusing on the catalytic applications of MOF/COF hybrids examined their utilization in photocatalysis. One of the initial reports on the photocatalytic activity of a MOF/COF hybrid showed that NH_2-MIL-68@TPA-COF provided 1.4 times enhanced photocatalytic activity for the degradation of rhodamine B compared to NH_2-MIL-68 due to increased surface area and smaller band gap of the hybrid compared to the pristine MOF.[35]

Multivariate Ti-MOF/COF hybrids, PdTCPP⊂PCN-415(NH_2)/TpPa, (where ⊂ symbolizes tetratopic porphyrin ligand incorporated into the MOF, PCN-415(NH_2), covalently connected to the COF, TpPa) were synthesized to combine the photocatalytic performance of Pd-porphyrin ligand with good light harvesting ability of TpPa. As shown in Fig. 2(a), the hybrids represented by 1, 2, and 3 which contain different amounts of the MOF offer performances better than pristine TpPA and several pristine MOF- and COF-based

photocatalysts for H_2 production (~14 mmol g^{-1} h^{-1} for composite 2) in the presence of a Pt cocatalyst.[50] Integration of Pd-porphyrin ligand into the MOF provided effective optical response, desirable band gap, and large surface area, in addition to high chemical stability.

A core–shell MOF@COF (a MOF in the core covered with a COF shell at the outer layer) system has been shown to be effective as a shape and size-selective catalyst for olefin separation.[38] Pd nanoparticles, mainly responsible for the catalytic activity, were sandwiched between the porous structure of the MOF, UiO-66-NH_2 in the core, and the selective COF-1 layer in the outer shell as shown in Fig. 2(b). COF-1 shell in the Pd/UiO-66-NH_2@COF heterogeneous catalytic platform enabled the diffusion of cyclohexene and trans-stilbene to interact with Pd sites immersed in the MOF and hindered the passage of larger triphenylethylene, leading to selective hydrogenation of cyclohexene and trans-stilbene as shown in Fig. 2(b). Zhao and coworkers showed that functionalizing the surface of a MOF with aldehyde (–CHO) groups provides more reacting sites for the growth of the COF shell, and such that the morphology of the shell layer could be designed as ultra-thin COF nanobelt or fibrillar-like.[51] The morphology of the shell layer affects the surface area, the number of active sites and migration of substrates. Therefore, depending on the morphology of the shell layer the performance of the MOF@COF catalyst could be arranged while Pd nanoparticles dispersed on the nanobelt shell layer facilitated the trapping and flow of electrons during photocatalysis. As a result, Pd decorated Ti-MOF@TpTt catalyst shown in Fig. 2(c) has shown >99% conversion with >99% selectivity for the one-pot cascade hydrogenation of nitrobenzene using ammonia borane as the hydrogen source.

Finding efficient photocatalysts for CO_2 reduction reaction is an ongoing challenge. Qizhao and coworkers obtained three different MOF/COF hybrid photocatalysts by combining the COF, TP-TA, with MOFs, NH_2-UiO-66(Zr), NH_2-MIL-101(Fe), or NH_2-MIL-68(In) and the highest photocatalytic CO_2 reduction rate belonged to NH_2-MIL-68(In)@TP-TA (leading to CO and CH_4 production rates of 25 and 11.67 μmol g^{-1} h^{-1}, respectively) due to its more negative conduction band potential compared to other two hybrid photocatalysts.[52] In another work, NH_2-UiO-66(Zr) was combined with an olefin-linked COF, TTCOF, and the heterojunction photocatalyst has shown a CO yield of 6.56 μmol g^{-1} h^{-1}, 4.4 and 5 times higher than the pristine COF and MOF, respectively. This is because the hybrid photocatalyst has provided an increased surface area (900 m^2 g^{-1}) which enhanced the transport of photogenerated carriers and their redox ability.[53] A hollow carbon electrocatalyst, Pt-COF@MOF$_{800}$, was obtained through the pyrolysis of TP-BPY-COF@ZIF-8 and showed enhanced catalytic conversion and selectivity due to smooth mass transport and large number of active sites for oxygen reduction reaction. Moreover, the hollow carbon electrocatalyst preserved its long-term stability both in alkaline and acidic environments.[54]

The covalent bond in MOF/COF hybrids is mostly responsible for the electron transfer in various catalytic reactions and it is also one of the challenges limiting the development of new MOF/COF hybrids since each MOF and COF cannot form covalently bound composites. To overcome this challenge, Yan and coworkers proposed post-synthetic modification to functionalize MOF-808, which does not have –NH$_2$ groups.[51] The core–shell structure of the covalently linked MOF-808@TpPa-1-COF obtained from NH$_2$-grafted MOF-808 and TpPa-1 showed an 11 mmol g^{-1} h^{-1} H$_2$ evolution rate for H$_2$ evolution reaction, almost 6 times higher than that of the pristine COF. The composite without the covalent link (MOF-808/TpPa-1-COF) showed a H$_2$ evolution rate of 4.51 mmol g^{-1} h^{-1}, highlighting the importance of the covalent link for efficient charge separation and transport.[51] Most of these early efforts focused on the same type of MOFs and COFs to generate and test MOF/COF hybrids as catalysts. Considering the very large number of MOF–COF combinations, there is a vast space of opportunity for designing new MOF/COF hybrids that can offer outstanding catalytic performances.

Membrane-based gas separation

In this section, we consider membrane-based gas separation applications as a part of energy-related applications since membranes have been widely investigated to separate industrially important gas mixtures, such as CO$_2$ separation from flue gas which is critical to reduce global warming or CO$_2$ separation from natural gas which is critical to purify methane as an energy source. The first MOF/COF composite membrane was tested for H$_2$/CO$_2$ separation.[34] To fabricate COF-300/Zn$_2$(bdc)$_2$(dabco) and COF-300/ZIF-8 composite membranes, MOFs were grown on COF membranes, resulting in uniform layers of MOFs on the COF layer. The composite membranes showed higher H$_2$/CO$_2$ selectivities (~13) than selectivities of the pristine MOF (7–9) and COF (6) membranes and surpassed the Robeson's upper bound.[55] The presence of an amorphous MOF layer shown in Fig. 3 was attributed to the dissimilarity in the lattice parameters of MOFs and COFs which caused the disorder at the initial stage of the nucleation of MOF crystals. The amorphous layer enhanced the interaction of MOF and COF at the interface and enabled the selective passage of H$_2$ molecules due to the smaller kinetic diameter of H$_2$ (2.9 Å) compared to that of CO$_2$ (3.3 Å). Das and Ben fabricated a COF-300/UiO-66 composite membrane for H$_2$/CO$_2$ separation.[56] The COF-300/UiO-66 composite showed a remarkable separation performance (H$_2$/CO$_2$ selectivities of 24 and 17 for single-gas and binary mixture conditions, respectively) and outperformed the H$_2$/CO$_2$ mixture selectivities of COF-300/Zn$_2$(bdc)$_2$(dabco) (12.6) and COF-300/ZIF-8 (13.5) composite membranes. The improvement in H$_2$/CO$_2$ selectivity of the composite membrane was attributed to the interfacial interactions between the Zn cation of MOF and amine group of COF layers.

Since the current membrane market is dominated by polymers due to their low cost and good processability, MOF@COF hybrids (UiO-66-NH$_2$@TpPa-1) were used as fillers in a polymer matrix, polysulfone (PSf), to generate a mixed matrix membrane (MMM) for separation of equimolar CO$_2$/CH$_4$ mixture.[37] When 5 wt% of MOF@COF filler was added into the PSf (CO$_2$ permeability: ~5 Barrer, CO$_2$/CH$_4$ selectivity: 26), the resulting MMM exhibited 48% and 79% improvements in CO$_2$ permeability (7 Barrer) and CO$_2$/CH$_4$ selectivity (47), respectively, compared to pristine PSf, in addition to good operational stability. Particle agglomeration and interfacial voids did not occur at low wt% of the MOF@COF filler (<10 wt%) due to the good adhesion between the polymer matrix and the COF coating layer, suggesting improved interface compatibility. Thus, using
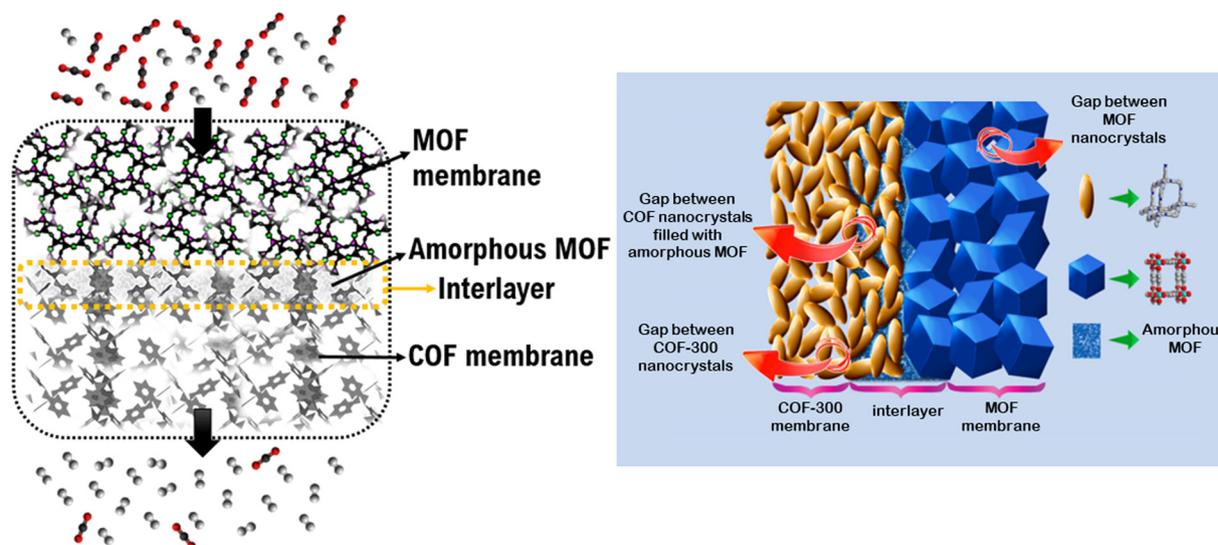

Fig. 3 Schematic representation of MOF/COF composite membrane. The amorphous MOF formed in the interlayer filled the free spaces between COF crystals and the interface between COF and MOF layers. The figure was adapted from the literature with permission from ref. 34. Copyright (2016) American Chemical Society.

MOF@COF hybrids as fillers in polymers is useful not only to obtain improved permeability and selectivity compared to pristine polymer but also to fabricate defect-free membranes with enhanced compatibility at the polymer-filler interface.

Nano-agents and biosensors

Nanoscale agents are generally used to deliver photosensitizers (molecular agents that destruct the tumor upon exposure to light) to target tissues since it is challenging to find photosensitizer molecules that are water-soluble (for high cell uptake) and able to bind selectively to tumor tissues with various characteristics.[57] MOFs and COFs with high porosity, large surface area, high tunability are potential nano-carriers for the treatment of sick tissue since their properties facilitate the transport of photosensitizers via different routes.[16,58] Still, it is necessary to increase the responsiveness of these nano-carriers specifically to the tumor tissue while also monitoring their size, stability, blood half-life, and removal from the body.[59] Zheng and coworkers synthesized photoactive amine containing UiO-66-based hybrids (MOF@amorphous COF system) for photodynamic therapy applications. When the hybrids were exposed to light irradiation, they showed high phototoxicities against human hepatocellular carcinoma (HepG2) and HeLa cells, suggesting that these hybrids can be effectively used for cancer treatment.[60] Here, selection of porphyrin-based structures is important since they produce cytotoxic reactive oxygen species for photodynamic therapy. Recently, the same group examined another hybrid material by using Hf-UiO-AM MOF and a chlorine-based amorphous COF modified with polyethylene glycol. Hf-UiO-AM@POP-PEG (HUC–PEG) composite provided a superior antitumor activity by producing O_2 due to improved light harvesting ability.[61] The interface formed by the MOF and the amorphous COF provided the composite with high photodynamic and photothermal efficiency. Therefore, the MOF@amorphous COF system is considered as a biocompatible and efficient nano-agent fulfilling the important prerequisites of biomedical applications.[62] This study revealed that the interface-based design of composite materials is highly useful to control the photochemical environment in porous media.

Recently, MOF@COF hybrids were utilized as nanozymes for enhanced bacterial inhibition.[39] Amino-functionalized peroxidase-like NH_2-MIL-88B(Fe) was synthesized and then grafted with COF-TP-TTA. Constructed nanocavities with functional surfaces acted as enzyme binding pockets to activate substrate molecules like H_2O_2 through non-covalent interactions. The surface chemistry and morphology of the MOF@COF hybrid served as a platform to catch and kill the bacteria. This study presented the potential of MOF/COF hybrids to mimic nature-inspired nanozymes and construct biosensors for the target molecules, inhibit bacterial growth, and promote wound healing in nanomedicine.

Biosensors are considered as an interesting nanomedical application of MOF/COF hybrids. Aptamer-based electrochemical biosensors have been developed since they have the recognition ability to detect molecules of interest. To enhance the sensitivity of the electrochemical aptamer-based sensors, MOF@COF hybrids were used to modify the electrode.[63] Liu and coworkers synthesized the Co-MOF@TPN-COF hybrid for the detection of the widely used β-lactam antibiotics, ampicillin from human serum, river water, and milk.[36] Nitrogen-based functional group triazine in TPN-COF enhanced the interaction between aptamer strands and Co-MOF@TPN-COF. The composite had a superior electrochemical performance compared to pristine MOF and COF, and provided a very low detection limit (0.271 fg mL^{-1}) toward ampicillin, resulting in an ultra-sensitive sensor in addition to its excellent stability and reproducibility. Xu and coworkers fabricated a Cu-MOF@CuPc-TA-COF hybrid as a photoelectrochemical biosensor for detecting HIV-1.[42] The material provided high selectivity towards HIV-1 target DNA (tDNA), good reproducibility, and superior stability. Aptamer strands (single-strand DNA or RNA) trigger the electrochemical activity of the sensor, and due to the strong molecular interactions between aptamer strands and the hybrids, including electrostatic, π–π stacking, and hydrogen bonding, aptamer immobilization and antibiotic adsorption were enhanced. Zhang et al. developed a novel biosensor based on the CoPc-PT-COF@Cu-MOF hybrid to detect Cr^{3+} ions from the aqueous environment. Since the composite had a high surface area, a mixed metal content (Co and Cu), and amino functional groups, it offered an enhanced photoelectrochemical activity and therefore a better bio-affinity towards DNA strands compared to its pristine pairs.[64] All these pioneering works highlight the synergistic effects raised by the combination of MOF and COF structures to construct biosensors for target molecules.

Adsorption

When MOFs and COFs are combined to fabricate MOF/COF hybrids, adsorbent capacity could be improved. For example, Wang and coworkers assembled COF-1 and MOF-235/MIL-88 type MOFs using pore-space-partition strategy, the rational fractionation of the large pore space of MOFs to maximize the host–guest interactions. The resulting hybrid materials provided higher C_2H_2, C_2H_4, C_2H_6, CH_4, CO_2, and NH_3 uptakes compared to their pristine forms.[65] Garzón-Tovar et al. synthesized a MOF/COF (UiO-66-NH_2/COF-1,3,5-tris-(4-aminophenyl)benzene (TAPB) and 1,3,5-benzenetricarbaldehyde (BTCA)) composite by confining MOF particles in single spherical COF beads.[66] Additional pores occurred at the MOF/COF interface resulting in a synergistic increase in both N_2 and H_2O uptakes compared to their constituent pairs. Similarly, due to ultramicropores created at the interfacial layer of NH_2-UiO-66 and Br-COF, CO_2 uptake of NH_2-UiO-66@Br-COF (169.5 mg g^{-1}) was found to be much higher than that of pristine NH_2-UiO-66 (149.5 mg g^{-1}) and Br-COF (50.0 mg g^{-1}) adsorbents measured at 273 K and 1

bar.[67] The additional nitrogen sites introduced in the NH_2-UiO-66@Br-COF composite provided strong acid–base and dipole–quadrupole interactions with CO_2 molecules. Therefore, new adsorption sites were created by the combination of MOF and COF structures, which eventually led to enhanced gas adsorption.

Energy storage

MOF/COF hybrid-based electrode materials have recently been considered for high-performance supercapacitor applications. Pristine MOFs and COFs generally have low electrical conductivities, which hinder their use in energy storage applications. Therefore, redox active molecules like 7,7,8,8-tetracyanoquinodimethane (TCNQ) can be incorporated within nanoporous materials to improve their electrical conductivity. For example, recently a redox-active TCNQ molecule was incorporated into the pores of a MOF@COF hybrid. Uniform pores enhanced the diffusion of ions and redox-active sites obtained with the introduction of TCNQ molecule enhanced the quantum capacitance of the resulting hybrid material which exhibited an excellent supercapacitor performance.[68]

Another energy storage application of MOF/COF hybrids is lithium–sulfur (Li–S) batteries, which consist of a Li anode and an S cathode. Li–S batteries are promising battery types due to their high energy densities.[69] Loss of cycle stability due to the shuttling of lithium polysulfides and slow sulfur reaction kinetics due to poor conductivity of sulfur are the main problems that hinder the industrial applications of Li–S batteries.[70] Lin et al. utilized the core–shell structure of MOF/COF hybrids to overcome the shuttling of lithium polysulfides in Li–S batteries and discovered TpPa-1 coated MOF-derived N-doped carbon (TpPa-1 coated UiO-66-NH_2 derived Co/Zr-NC).[43] ZrO_2 and Co nanoparticles within the NC contributed to the trapping of polysulfides while the NC itself provided the enhanced conductivity of the composite. COF coating layer succeeded to avoid the shuttling effect by providing selective penetration of Li^+ ions through the channels with effective sulfur trapping. These studies emphasized the importance of post-synthetic modification of MOF/COF hybrids for energy storage applications.

Chemical sensing

MOF/COF composites were examined for the detection and removal of metal ions, pesticides, or endocrine-disrupting chemical agents such as bisphenols. Solid-phase extraction is an efficient method to detect and remove metal ions such as Cu^{2+}, Pb^{2+}, Li^+, Ag^+, Cd^{2+}, Mg^{2+}, and Zn^{2+}, pesticides, and endocrine-disrupting agents while the use of magnetic nanomaterials facilitates the extraction of these agents.[71] Li et al. showed that Fe_3O_4 incorporated UiO-66-NH_2@TpBD composites selectively separate trace copper (Cu^{2+}) from water due to the magnetic property introduced by Fe_3O_4 particles in MOF and extra adsorption sites introduced by the oxygen and nitrogen-containing organic groups of the COF.[72]

The Fe_3O_4@MOF@COF composite in magnetic solid phase extraction of Cu^{2+}, and Cu^{2+} catalyzed oxidation reaction monitored by UV-vis spectrophotometry has shown to be a facile, stable, and selective platform for the detection of trace amount of Cu in environmental samples. Similarly, the composite of IRMOF-3 and TpBD has shown an excellent dual functionality of Pb^{2+} detection and fluorescence sensing of a nitro-explosive in water samples.[73]

Zhao and coworkers coupled ZIF-8 with Fe_3O_4 incorporated COF, Fe_3O_4@TAPB, and Fe_3O_4@TAPB@ZIF-8 nanocomposites were used for the selective detection of bisphenols in food samples.[74] π–π stacking interactions, hydrophilicity, polarity, and hydrogen bonding interactions were the main contributors to the adsorption efficiency of the nanocomposite. UiO-66-NH_2@TpBD composites immobilized on carboxyl cotton fibers were studied for bisphenol detection and shown to be reusable and reproducible with high adsorption capacity.[75] Similarly, UiO-66@COF-V composites were found to be highly effective for the detection of trace phenoxy carboxylic acids in water and vegetables (a highly toxic pesticide for living organisms) due to the π–π interactions, hydrogen bonding, and halogen bonds.[76] These studies indicate that MOF@COF composites already commit a high monitoring performance to be used in chemical sensing of pollutants in food and water samples and new hybrids would extend their limits.

3. Computational investigation of MOF/COF hybrids

Investigation of MOF/COF hybrids is accelerated in recent years but very little number of studies utilized computational tools for the design of these hybrids or to predict their performances for different applications. The literature on MOF/COF hybrids has also shown that so far only a limited number of MOFs and COFs are utilized to generate MOF/COF hybrids while numerous MOF and COF candidates are awaiting to be discovered. At this point, computational studies would be very useful to select the best MOF and COF candidates among many to provide a road map for the synthesis of novel MOF/COF hybrids. Kim and coworkers followed a three-step methodology, matching of lattice parameters of a MOF and a COF, identification of connection points, and translation of MOF and COF unit cells as shown in Fig. 4 to determine the interfacial compatibility of different MOFs and COFs. In the first step, the translational symmetry of the MOF and COF superlattices at the interface was compared and then nitrogen atoms in amine-functionalized MOFs and imine-based COFs were identified as the chemical connection points. Finally, the overlap of chemical connection points of the MOF and the COF was calculated while keeping the coordinates of the MOF atoms as fixed and translating the unit cell of the COF by 0.5 Å. Atomic site overlap was calculated at the last step to check how many chemical connection points of the COF are in enough vicinity with respect to the chemical connection
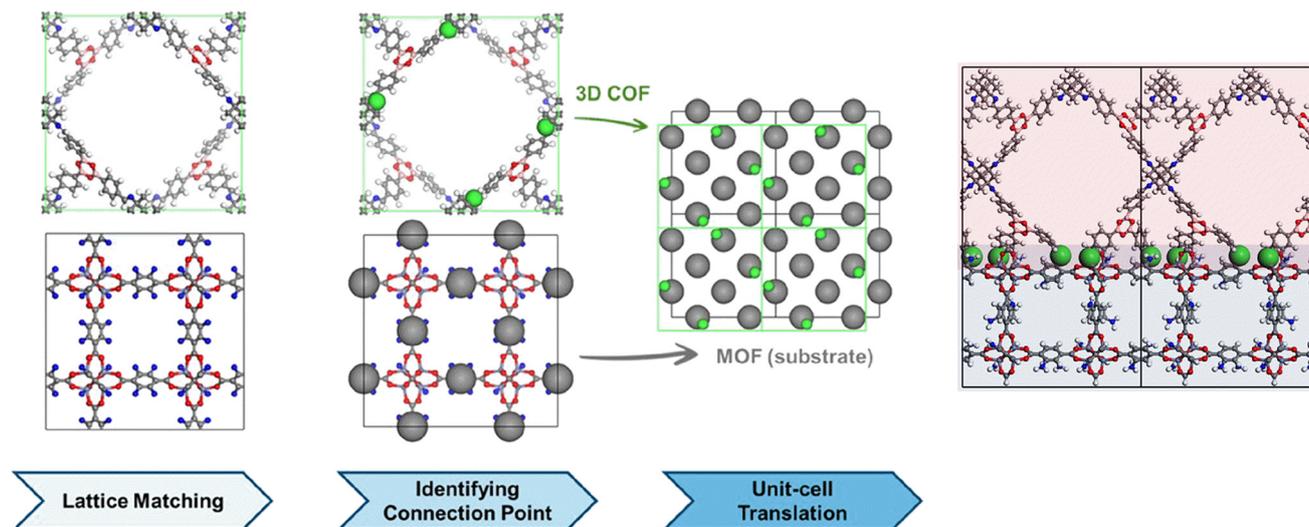
Fig. 4 Three steps for heteroepitaxial growth of 3D COFs on MOFs and the final structure. Reprinted with permission from ref. 40. Copyright (2021) American Chemical Society.

points of the MOF to make a connection. This computational approach to determine the synthesizable MOF/COF hybrids showed that among 537 amine-functionalized MOFs and 49 imine-based 3-dimensional COFs, it is possible to synthesize only 19 MOF/COF pairs.[40]

In another work, experimentally measured H_2 separation performance of a MOF/COF hybrid membrane was supported with computational investigation. Fan and co-workers developed a MOF-in-COF concept by locating a MOF, ZIF-67, inside a COF, TpPA-1, for H_2/CO_2 and H_2/CH_4 separations to benefit from the molecular sieving property of the MOF.[41] The unit cell size of ZIF-67 is close to the inner pore size of TpPA-1, therefore the pore of the COF can be used to locate the MOF as a cage as shown in Fig. 5(a). Results showed that ZIF-67-in-TpPA-1, ZIF-8-in-TpPA-1, and ZIF-67-in-TpBD membranes outperform traditional zeolites, MOFs, and POMs (polyoxometalates) by surpassing the upper bound established for H_2/CO_2 and H_2/CH_4 separations as shown in Fig. 5(b). The high H_2 permeability and selectivity were attributed to the creation of molecular sieving channels in the MOF-in-COF layer. For the computational investigation, one unit cell of ZIF-67 was incorporated into the pore of TpPa-1. To predict the mixture selectivity, TpPa-1 or ZIF-67-in-TpPA-1 membranes were placed in the middle of two chambers, one chamber containing an equimolar mixture of H_2/CO_2 or H_2/CH_4 and the other one is under vacuum, as shown in Fig. 5(c) and the system was optimized. Molecular dynamics (MD) simulations were then performed and the gas molecules were allowed to diffuse through the membrane. Although the simulation time was too short to compute the gas fluxes, the number of H_2, CO_2, and CH_4 molecules which penetrate through the membrane were depicted. Low CO_2 permeance was attributed to the slow diffusivity of CO_2 molecules due to their strong adsorption on the surface of ZIF-67 in TpPa-1. As a result, simulations suggested a higher

H_2/CO_2 selectivity than the H_2/CH_4 selectivity, complementing the experimental findings. This first MD simulation of MOF-in-COF layer opens the door for future work on developing new computational methodologies to further analyze the gas transport mechanism in MOF@COF, COF@MOF, and MOF-in-COF systems.

Electron-based calculations using density functional theory (DFT) were also employed to understand the enhanced photocatalytic performance of MOF/COF hybrids. Zhuang and coworkers grew ZIF-67 crystals on benzoic acid modified COF. The calcinated form of ZIF-67/COF composite (Co_3O_4/NPC) provided a good catalytic activity for oxygen evolution reaction, and high cycling stability and a reversible capacity for Li-ion battery applications.[77] DFT calculations were used to explain the most stable configuration for the adsorption of H_2O and O_2 on Co_3O_4/NPC during oxygen evolution reaction. Results showed that adsorption/desorption of reaction species was highly sensitive to the geometrical and electronic properties of the composite. Nitrogen atoms and unsaturated Co sites of Co_3O_4/NPC facilitated the activation of H_2O on Co_3O_4 and easy desorption of O_2. All these studies show that efficient use of computational methods can bring new insights not only for designing and discovering new MOF/COF hybrids for a target use, but also for understanding the mechanism behind the performance enhancement offered by MOF/COF hybrids.

4. Outlook

The research on MOF/COF hybrids is still ongoing and we expect to see more efforts that unravel the potential of MOF@COF, COF@MOF, and COF-in-MOF or MOF-in-COF composites for various applications. Considering the increasing number of studies on MOF/COF hybrids, we
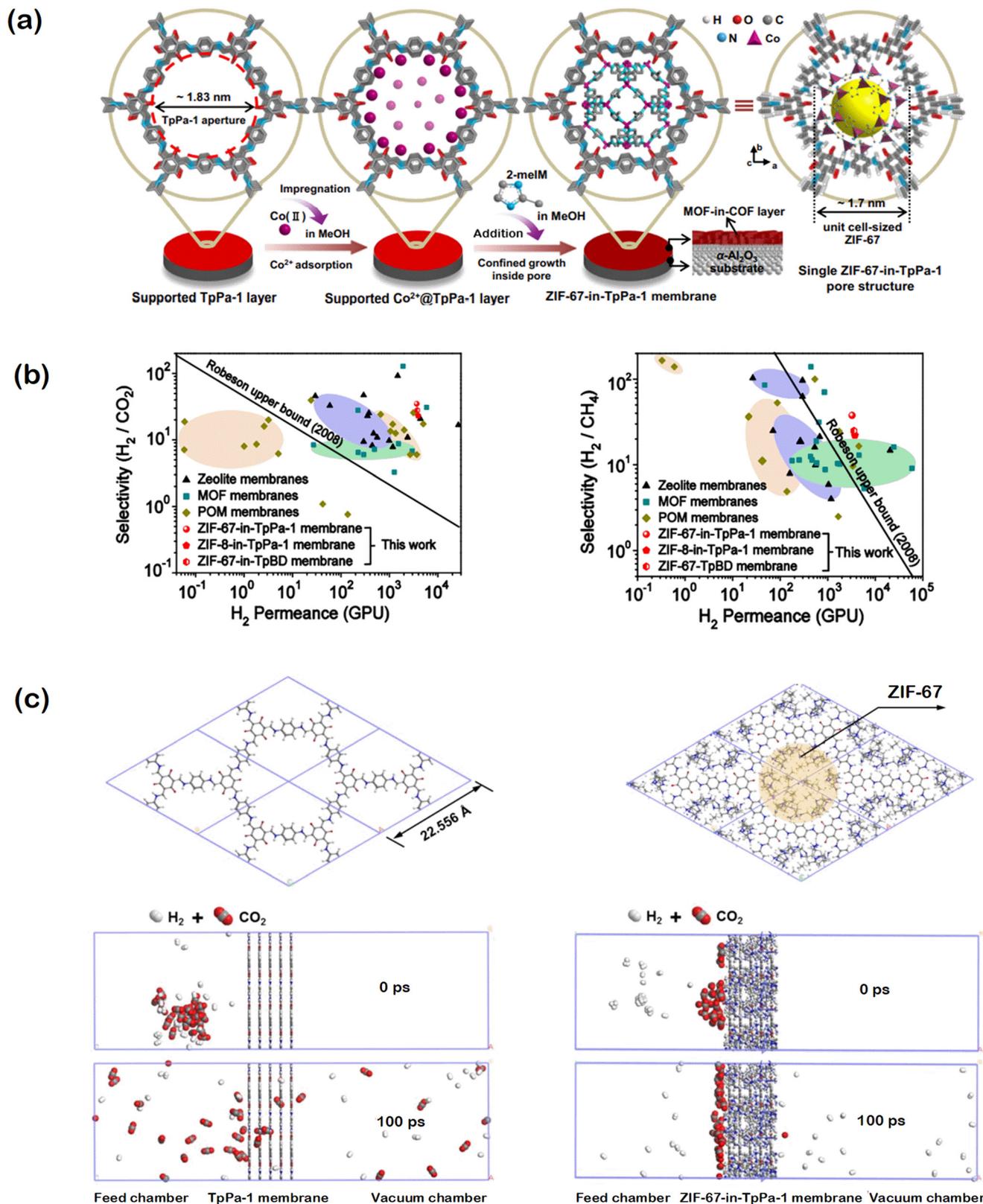
Fig. 5 (a) Representation of MOF-in-COF (ZIF-67-in-TpPa-1) structure. In the impregnation step, the supported TpPa-1 layer was immersed in cobalt nitrate hexahydrate solution and then 2-methylimidazole (2-meIm) solution. Reprinted with permission from ref. 41. (b) Comparison of H_2 permeance, H_2/ CO_2, and H_2/CH_4 selectivities of MOF-in-COF membranes with those of traditional membranes. Reprinted with permission from ref. 41. (c) Simulation system to depict H_2/CO_2 permeation through pure TpPa-1 membrane and ZIF-67 incorporated TpPa-1 membrane. Reprinted from ref. 41 under the terms of the CC BY licence **https://creativecommons.org/licenses/by/4.0/**.

believe the following directions would be important to further realize the efficient use of these hybrids:

Computational design of MOF/COF hybrids for specific targets

The enormous number of MOFs and COFs creates the illusion of a vast design space for MOF–COF heterostructures, while a limited number of MOF and COF combinations have been experimentally examined to date since it is challenging to select the most appropriate MOF/COF combinations for a desired application. Previous research on MOF–COF heterostructures has revealed that due to compatibility concerns, mostly MOFs containing amine groups that covalently link with the imine-based COFs are utilized. Therefore, development of MOF/COF heterostructures would benefit greatly from guidelines that consider the crystal geometry, lattice matching, hydrophobicity, stability, flexibility, and functional groups of MOF and COF structures. It is important to note that hypothetical MOF and COF datasets,[78–81] consisting of computationally designed but not experimentally synthesized materials, also exist and can be further investigated to design hypothetical MOF/COF hybrids.

Structural characterization of MOF/COF hybrids

Comprehensive characterization methods are highly needed for the detailed understanding of the morphology of MOF/COF hybrids. The interfacial properties of MOFs and COFs have a particularly important role in determining the ultimate performance of hybrid materials. For example, atomic pair distribution function analysis, which reveals the local order of the amorphous and crystalline regions in nanomaterials, can be used to examine the interactions at the MOF/COF interface. At this point, theoretical investigation using computational tools, discussed solely in a few works,[41,77] will play an essential role by revealing the mechanism underlying the activity of MOF/COF hybrids in different applications and providing a solid understanding of their interfacial properties.

Developing structure–performance relations for MOF/COF hybrids

Numerous MOF/COF hybrids can be generated, while their efficient use for an application of interest depends on the properties of each component and their proportions in the hybrid. Developing structure–performance relationships will be useful and machine learning approaches are proven to be efficient in this manner.[82] For example, structural properties of MOFs and COFs, such as the pore size, surface area, porosity, chemical composition can be used as descriptors to train machine learning models that accurately predict the performances of MOF/COF hybrids for target applications. Machine learning approaches can also be used to predict synthesizability of novel MOF/COF hybrids with desired structural and chemical properties.

Combining MOF/COF hybrids with other materials

Covering the external surface of MOFs with a COF can provide good compatibility with the organic nature of the polymer for MMM applications. This is an emerging field which requires both experimental and computational works to understand the molecular-level interactions between MOF/COF hybrids and polymers that can lead to high-performance MMMs to replace the polymer membranes. In the last years, ionic liquids, molten salts in liquid form at room temperature, have been incorporated into MOFs and COFs to post-synthetically modify their pore environments which leads to enhanced gas separation and catalysis performances due to the strong molecular interactions between ionic liquids and adsorbate molecules.[83] Similarly, incorporating ionic liquids into MOF/COF hybrids to tune the pore shape/size and affinity towards target molecules can be another interesting venue. Advances in experimental and computational methodologies in the future will provide an in-depth insight into the design and development of new MOF/COF hybrids which can outperform pristine MOFs and COFs for various applications by combining the advantages of two material families.

Conflicts of interest

There are no conflicts to declare.

Acknowledgements

References

1 A. K. Cheetham, G. Ferey and T. Loiseau, *Angew. Chem., Int. Ed.*, 1999, **38**, 3268–3292.

2 B. Cui and G. Fu, *Nanoscale*, 2022, **14**, 1679–1699.

3 Y. Shan, L. Chen, H. Pang and Q. Xu, *Small Struct.*, 2020, **2**, 2000078.

4 S. R. Batten, N. R. Champness, X. M. Chen, J. Garcia-Martinez, S. Kitagawa, L. Ohrstrom, M. O'Keeffe, M. P. Suh and J. Reedijk, *CrystEngComm*, 2012, **14**, 3001–3004.

5 O. M. Yaghi, H. L. Li, C. Davis, D. Richardson and T. L. Groy, *Acc. Chem. Res.*, 1998, **31**, 474–484.

6 H. Furukawa, N. Ko, Y. B. Go, N. Aratani, S. B. Choi, E. Choi, A. O. Yazaydin, R. Q. Snurr, M. O'Keeffe, J. Kim and O. M. Yaghi, *Science*, 2010, **329**, 424–428.

7 S. Kitagawa, R. Kitaura and S. Noro, *Angew. Chem., Int. Ed.*, 2004, **43**, 2334–2375.

8 Y. Cui, B. Li, H. He, W. Zhou, B. Chen and G. Qian, *Acc. Chem. Res.*, 2016, **49**, 483–493.

9 A. J. Howarth, Y. Y. Liu, P. Li, Z. Y. Li, T. C. Wang, J. Hupp and O. K. Farha, *Nat. Rev. Mater.*, 2016, **1**, 15018.

10   C. S. Diercks and O. M. Yaghi, *Science*, 2017, **355**, eaal1585.

11   J. Hu, S. K. Gupta, J. Ozdemir and M. H. Beyzavi, *ACS Appl. Nano Mater.*, 2020, **3**, 6239–6269.

12   H. Wang, Z. Zeng, P. Xu, L. Li, G. Zeng, R. Xiao, Z. Tang, D. Huang, L. Tang, C. Lai, D. Jiang, Y. Liu, H. Yi, L. Qin, S. Ye, X. Ren and W. Tang, *Chem. Soc. Rev.*, 2019, **48**, 488–516.

13   D. G. Wang, T. J. Qiu, W. H. Guo, Z. B. Liang, H. Tabassum, D. G. Xia and R. Q. Zou, *Energy Environ. Sci.*, 2021, **14**, 688–728.

14   A. P. Cote, A. I. Benin, N. W. Ockwig, M. O'Keeffe, A. J. Matzger and O. M. Yaghi, *Science*, 2005, **310**, 1166–1170.

15   H. Wang, H. Wang, Z. Wang, L. Tang, G. Zeng, P. Xu, M. Chen, T. Xiong, C. Zhou, X. Li, D. Huang, Y. Zhu, Z. Wang and J. Tang, *Chem. Soc. Rev.*, 2020, **49**, 4135–4165.

16   L. L. Feng, C. Qian and Y. L. Zhao, *ACS Mater. Lett.*, 2020, **2**, 1074–1092.

17   R. Freund, O. Zaremba, G. Arnauts, R. Ameloot, G. Skorupskii, M. Dinca, A. Bavykina, J. Gascon, A. Ejsmont, J. Goscianska, M. Kalmutzki, U. Lachelt, E. Ploetz, C. S. Diercks and S. Wuttke, *Angew. Chem., Int. Ed.*, 2021, **60**, 23975–24001.

18   S. Abednatanzi, M. Najafi, P. G. Derakhshandeh and P. Van Der Voort, *Coord. Chem. Rev.*, 2022, **451**, 214259.

19   P. Z. Moghadam, A. Li, S. B. Wiggin, A. Tao, A. G. P. Maloney, P. A. Wood, S. C. Ward and D. Fairen-Jimenez, *Chem. Mater.*, 2017, **29**, 2618–2625.

20   D. Ongari, A. V. Yakutovich, L. Talirz and B. Smit, *ACS Cent. Sci.*, 2019, **5**, 1663–1675.

21   D. Ongari, L. Talirz and B. Smit, *ACS Cent. Sci.*, 2020, **6**, 1890–1900.

22   Y. G. Chung, E. Haldoupis, B. J. Bucior, M. Haranczyk, S. Lee, H. D. Zhang, K. D. Vogiatzis, M. Milisavljevic, S. L. Ling, J. S. Camp, B. Slater, J. I. Siepmann, D. S. Sholl and R. Q. Snurr, *J. Chem. Eng. Data*, 2019, **64**, 5985–5998.

23   Z. Chen, X. Li, C. Yang, K. Cheng, T. Tan, Y. Lv and Y. Liu, *Adv. Sci.*, 2021, **8**, e2101883.

24   Y. Li, M. Karimi, Y. N. Gong, N. Dai, V. Safarifard and H. L. Jiang, *Matter*, 2021, **4**, 2230–2265.

25   M. C. Ma, X. F. Lu, Y. Guo, L. C. Wang and X. J. Liang, *TrAC, Trends Anal. Chem.*, 2022, **157**, 116741.

26   G. Yuan, L. Tan, P. Wang, Y. Wang, C. Wang, H. Yan and Y.-Y. Wang, *Cryst. Growth Des.*, 2021, **22**, 893–908.

27   C. Zhang, B. H. Wu, M. Q. Ma, Z. Wang and Z. K. Xu, *Chem. Soc. Rev.*, 2019, **48**, 3811–3841.

28   M. Firoozi, Z. Rafiee and K. Dashtian, *ACS Omega*, 2020, **5**, 9420–9428.

29   C. Guo, F. Duan, S. Zhang, L. He, M. Wang, J. Chen, J. Zhang, Q. Jia, Z. Zhang and M. Du, *J. Mater. Chem. A*, 2022, **10**, 475–507.

30   Y. Deng, Y. Wang, X. Xiao, B. J. Saucedo, Z. Zhu, M. Xie, X. Xu, K. Yao, Y. Zhai, Z. Zhang and J. Chen, *Small*, 2022, **18**, 2202928.

31   J. Wang, Y. Q. Feng and B. Zhang, *Prog. Chem.*, 2022, **34**, 1308–1320.

32   M. X. Wu, Y. Wang, G. H. Zhou and X. M. Liu, *Coord. Chem. Rev.*, 2021, **430**, 213735.

33   S. Zhang, F. L. Rong, C. A. P. Guo, F. H. Duan, L. H. He, M. H. Wang, Z. H. Zhang, M. M. Kang and M. Du, *Coord. Chem. Rev.*, 2021, **439**, 213948.

34   J. Fu, S. Das, G. Xing, T. Ben, V. Valtchev and S. Qiu, *J. Am. Chem. Soc.*, 2016, **138**, 7673–7680.

35   Y. Peng, M. Zhao, B. Chen, Z. Zhang, Y. Huang, F. Dai, Z. Lai, X. Cui, C. Tan and H. Zhang, *Adv. Mater.*, 2018, **30**, 1705454.

36   X. Liu, M. Hu, M. Wang, Y. Song, N. Zhou, L. He and Z. Zhang, *Biosens. Bioelectron.*, 2019, **123**, 59–68.

37   Y. D. Cheng, Y. P. Ying, L. Z. Zhai, G. L. Liu, J. Q. Dong, Y. X. Wang, M. P. Christopher, S. C. Long, Y. X. Wang and D. Zhao, *J. Membr. Sci.*, 2019, **573**, 97–106.

38   W. Q. Zhou, Y. Liu, W. L. Teo, B. Chen, F. C. Jin, L. Y. Zhang, Y. F. Zeng and Y. L. Zhao, *Cell Rep. Phys. Sci.*, 2020, **1**, 100272.

39   L. Zhang, Z. Liu, Q. Deng, Y. Sang, K. Dong, J. Ren and X. Qu, *Angew. Chem., Int. Ed.*, 2021, **60**, 3469–3474.

40   H. Park, O. Kwon and J. Kim, *J. Phys. Chem. C*, 2021, **125**, 5897–5903.

41   H. Fan, M. Peng, I. Strauss, A. Mundstock, H. Meng and J. Caro, *Nat. Commun.*, 2021, **12**, 38.

42   M. Xu, K. Chen, L. Zhu, S. Zhang, M. Wang, L. He, Z. Zhang and M. Du, *Langmuir*, 2021, **37**, 13479–13492.

43   T. Y. Lin, H. Y. Wang, X. H. Du, D. S. Zhang, Z. S. Zhang and G. H. Liu, *Electrochim. Acta*, 2022, **412**, 140156.

44   U. Mueller, M. Schubert, F. Teich, H. Puetter, K. Schierle-Arndt and J. Pastre, *J. Mater. Chem.*, 2006, **16**, 626–636.

45   K. Schlichte, T. Kratzke and S. Kaskel, *Microporous Mesoporous Mater.*, 2004, **73**, 81–88.

46   S. Y. Ding, J. Gao, Q. Wang, Y. Zhang, W. G. Song, C. Y. Su and W. Wang, *J. Am. Chem. Soc.*, 2011, **133**, 19816–19822.

47   M. Lu, M. Zhang, J. Liu, Y. Chen, J. P. Liao, M. Y. Yang, Y. P. Cai, S. L. Li and Y. Q. Lan, *Angew. Chem., Int. Ed.*, 2022, **61**, e202200003.

48   L. Fan, Z. Kang, M. Li and D. Sun, *Dalton Trans.*, 2021, **50**, 5732–5753.

49   Z. Song, L. Zhang, K. Doyle-Davis, X. Fu, J. L. Luo and X. Sun, *Adv. Energy Mater.*, 2020, **10**, 2001561.

50   C. X. Chen, Y. Y. Xiong, X. Zhong, P. C. Lan, Z. W. Wei, H. Pan, P. Y. Su, Y. Song, Y. F. Chen, A. Nafady, S/O G. M. Sirajuddin and S. Ma, *Angew. Chem., Int. Ed.*, 2022, **61**, e202114071.

51   M. Y. Zhang, J. K. Li, R. Wang, S. N. Zhao, S. Q. Zang and T. C. W. Mak, *Adv. Sci.*, 2021, **8**, e2101884.

52   L. Wang, J. X. Mao, G. F. Huang, Y. Zhang, J. W. Huang, H. D. She, C. L. Liu, H. Liu and Q. Z. Wang, *Chem. Eng. J.*, 2022, **446**, 137011.

53   Q. Niu, S. Dong, J. Tian, G. Huang, J. Bi and L. Wu, *ACS Appl. Mater. Interfaces*, 2022, **14**, 24299–24308.

54   Y. Guo, S. Yang, Q. Xu, P. Wu, Z. Jiang and G. F. Zeng, *J. Mater. Chem. A*, 2021, **9**, 13625–13630.

55   L. M. Robeson, *J. Membr. Sci.*, 2008, **320**, 390–400.

56   S. Das and T. Ben, *Dalton Trans.*, 2018, **47**, 7206–7212.

57   J. Liu, J. Shi, W. Nie, S. Wang, G. Liu and K. Cai, *Adv. Healthcare Mater.*, 2021, **10**, e2001207.

58 Y. Sakamaki, J. Ozdemir, Z. Heidrick, O. Watson, H. R. Shahsavari, M. Fereidoonnezhad, A. R. Khosropour and M. H. Beyzavi, *Comments Inorg. Chem.*, 2018, **38**, 238–293.

59 J. Feng, W. X. Ren, F. Kong and Y. B. Dong, *Inorg. Chem. Front.*, 2021, **8**, 848–879.

60 X. H. Zheng, L. Wang, Q. Pei, S. S. He, S. Liu and Z. G. Xie, *Chem. Mater.*, 2017, **29**, 2374–2381.

61 X. Zheng, L. Wang, Y. Guan, Q. Pei, J. Jiang and Z. Xie, *Biomaterials*, 2020, **235**, 119792.

62 E. K. Lim, T. Kim, S. Paik, S. Haam, Y. M. Huh and K. Lee, *Chem. Rev.*, 2015, **115**, 327–394.

63 H. W. Zhang, Q. Q. Zhu, R. R. Yuan and H. M. He, *Sens. Actuators, B*, 2021, **329**, 129144.

64 S. Zhang, K. Chen, L. Zhu, M. Xu, Y. Song, Z. Zhang and M. Du, *Dalton Trans.*, 2021, **50**, 14285–14295.

65 Y. Wang, X. Zhao, H. Yang, X. Bu, Y. Wang, X. Jia, J. Li and P. Feng, *Angew. Chem., Int. Ed.*, 2019, **58**, 6316–6320.

66 L. Garzón-Tovar, J. Pérez-Carvajal, A. Yazdi, J. Hernández-Muñoz, P. Tarazona, I. Imaz, F. Zamora and D. Maspoch, *Angew. Chem.*, 2019, **131**, 9612–9616.

67 J. Wang, L. Wang, Y. Wang, F. Yang, J. Li, X. Guan, J. Zong, F. Zhou, J. Huang and Y.-N. Liu, *Chem. Eng. J.*, 2022, **438**, 135555.

68 H. Peng, S. Huang, D. Tranca, F. Richard, W. Baaziz, X. Zhuang, P. Samori and A. Ciesielski, *ACS Nano*, 2021, **15**, 18580–18589.

69 Z. W. Seh, Y. Sun, Q. Zhang and Y. Cui, *Chem. Soc. Rev.*, 2016, **45**, 5605–5634.

70 O. Ogoke, G. Wu, X. L. Wang, A. Casimir, L. Ma, T. P. Wu and J. Lu, *J. Mater. Chem. A*, 2017, **5**, 448–469.

71 H. L. Jiang, N. Li, L. Cui, X. Wang and R. S. Zhao, *TrAC, Trends Anal. Chem.*, 2019, **120**, 115632.

72 W. T. Li, W. Shi, Z. J. Hu, T. Yang, M. L. Chen, B. Zhao and J. H. Wang, *Appl. Surf. Sci.*, 2020, **530**, 147254.

73 W. T. Li, Z. J. Hu, J. Meng, X. Zhang, W. Gao, M. L. Chen and J. H. Wang, *J. Hazard. Mater.*, 2021, **411**, 125021.

74 H. L. Jiang, Q. B. Fu, M. L. Wang, J. M. Lin and R. S. Zhao, *Food Chem.*, 2021, **345**, 128841.

75 X. Xu, N. Zhang, Y. Gao, T. Bao and S. Wang, *J. Environ. Chem. Eng.*, 2022, **10**, 107072.

76 Q. Fu, B. Sun, J. Fan, M. Wang, X. Sun, G. I. Waterhouse, P. Wu and S. Ai, *Food Chem.*, 2022, **371**, 131090.

77 G. L. Zhuang, Y. F. Gao, X. Zhou, X. Y. Tao, J. M. Luo, Y. J. Gao, Y. L. Yan, P. Y. Gao, X. Zhong and J. G. Wang, *Chem. Eng. J.*, 2017, **330**, 1255–1264.

78 C. E. Wilmer, M. Leaf, C. Y. Lee, O. K. Farha, B. G. Hauser, J. T. Hupp and R. Q. Snurr, *Nat. Chem.*, 2012, **4**, 83–89.

79 Y. J. Colón, D. A. Gomez-Gualdron and R. Q. Snurr, *Cryst. Growth Des.*, 2017, **17**, 5801–5810.

80 D. A. Gómez-Gualdrón, Y. J. Colón, X. Zhang, T. C. Wang, Y.-S. Chen, J. T. Hupp, T. Yildirim, O. K. Farha, J. Zhang and R. Q. Snurr, *Energy Environ. Sci.*, 2016, **9**, 3279–3289.

81 R. Mercado, R. S. Fu, A. V. Yakutovich, L. Talirz, M. Haranczyk and B. Smit, *Chem. Mater.*, 2018, **30**, 5069–5086.

82 K. M. Jablonka, D. Ongari, S. M. Moosavi and B. Smit, *Chem. Rev.*, 2020, **120**, 8066–8129.

83 O. Durak, M. Zeeshan, N. Habib, H. C. Gulbalkan, A. A. A. M. Alsuhile, H. P. Caglayan, S. F. Kurtoglu-Oztulum, Y. X. Zhao, Z. P. Haslak, A. Uzun and S. Keskin, *Microporous Mesoporous Mater.*, 2022, **332**, 111703.